ISSN: 2229-6956 (ONLINE)
DOI: 10.21917/ijsc.2025.0534

HYBRID DEEP LEARNING APPROACH FOR ENHANCED BRAIN TUMOR DETECTION IN BIOMEDICAL IMAGES USING SPARROW SEARCH OPTIMIZATION

V.Chanemougavel[1], K. Jayanthi[2] and A. Ganesh Prasannaa[3]

[1]Department of Computer and Information Science, Annamalai University, India
[2]Department of Computer Application, Government Arts College, Chidambaram, India
[3]Department of Computer Science and Engineering, Sai Ram Engineering College, India

Abstract

Brain tumours (BT) are considered one of the most aggressive and common diseases, leading to a short life expectancy. Therefore, timely and prompt treatment planning is the primary phase to progress the patient's quality of life. Usually, numerous image methods are employed to assess the cancer area in a brain. However, magnetic resonance imaging (MRI) is generally utilized owing to its higher image quality and trust in no ionizing radioactivity. The BT detection task by MRI was typically expensive and time-consuming for the specialists. So, computer-aided diagnosis (CAD)-based machine learning (ML) and deep learning (DL) are mainly progressed to perceive BTs early in less time without human involvement. This study proposes an Enhanced Detection of Brain Tumor Using Hybrid Model with Sparrow Search Algorithm (EDBT-HDLMSSA) approach. The proposed EDBT-HDLMSSA approach relies on improving the brain cancer recognition and classification model in biomedical images using advanced techniques. Initially, the image pre-processing applies a Sobel filter (SF) to eliminate the noise and skull removal using U-Net segmentation. Furthermore, the ShuffleNetv2.3 method is employed for feature extraction. The hybrid autoencoder and long short-term memory (AE-LSTM) method is implemented for the BT classification process. Finally, the hyperparameter selection of the AE-LSTM method is accomplished by utilizing the sparrow search algorithm (SSA) model. A wide range of experiments using the EDBT-HDLMSSA technique are achieved under the BT MRI dataset. The performance validation of the EDBT-HDLMSSA technique portrayed a superior accuracy value of 98.57% over existing models.

Keywords:

Brain Tumor, Hybrid Deep Learning Model, Sparrow Search Algorithm, Biomedical Imaging, Skull Removal

1. INTRODUCTION

BT is related to the combination of abnormal cells in a few brain tissues. Based on the beginning of BT, they are segmented into dual classes, metastatic and primary BTs [1]. The source of primary BT is in the brain, whereas metastasis begins from other organs. Cancer might be non- or cancerous [2]. Malignant BT grows quickly and infects other regions of the brain and spine, and in comparison with benign tumours, they are more severe. An elaborate cancer classification is divided into four grades; the higher-grade tumour is more malignant. Grade-I tumour cells are benign and almost normal in their presence [3]. Grade-II tumour cells arise to be slightly irregular. Grade-III tumour cells are malignant and abnormal. The most serious BTs comprising abnormal and fast-spreading cells are considered Grade-IV [4]. Early detection plays a central role in the therapy and retrieval of the patient. Usually, several image models like MRI, ultrasound image, and computed tomography (CT) are employed for assessing the BT [5].

MRI is the most prevalent non-invasive model. MRI's popularity originates from the reality of exploiting no ionizing radiation through the scan. Its higher soft-tissue resolution added the capability of attaining diverse images utilizing multiple image parameters or contrast-enhanced agents [6]. The classification phase might also be a tedious and confusing challenge for radiologists or physicians in a few complex situations [7]. This situation requires specialists to work on tumour localization, compare cancer tissues with neighbouring regions, utilize filters on the image if needed, make it more visible for human eyesight and eventually terminate [8]. These challenges are comparatively consuming more time, and that's why there is a necessity for a CAD method to timely identify BT in much less time without the involvement of humans. In former times, several ML methodologies are projected for cancer recognition utilizing MRI [9]. DL is a subset of ML that depends on hierarchical feature learning and learning representation of data. DL models employ a group of multiple layers of non-linear processing similarities for extracting features [10]. The output of every sequential layer is the input of another one and assists in data abstraction as we learn inside the system.

This study proposes an Enhanced Detection of Brain Tumor Using Hybrid Model with Sparrow Search Algorithm (EDBT-HDLMSSA) approach. The proposed EDBT-HDLMSSA approach relies on improving the brain cancer recognition and classification model in biomedical images using advanced techniques. Initially, the image pre-processing applies a Sobel filter (SF) to eliminate the noise and skull removal using U-Net segmentation. Furthermore, the ShuffleNetv2.3 method is employed for feature extraction. The hybrid autoencoder and long short-term memory (AE-LSTM) method is implemented for the BT classification process. Finally, the hyperparameter selection of the AE-LSTM method is accomplished by utilizing the sparrow search algorithm (SSA) model. A wide range of experiments using the EDBT-HDLMSSA technique are achieved under the BT MRI dataset.

2. RELATED WORKS

Abdusalomov et al. [11] study handles the complicated task of BT recognition in MRI scans utilizing a massive set of BT images. The authors have proven that fine-tuning an advanced YOLO-v7 technique over TL considerably improved its recognition performance. Poonguzhali et al. [12] developed an Automated Deep Residual U-Net Segmentation with a Classification model (ADRU-SCM) for diagnosing BT. The projected method is mainly aimed at the classification and segmentation of BT. Also, a wiener filter (WF) is used for image pre-processing. In addition, the VGG-19 method is used as a feature extractor. Solanki et al. [13] demonstrate an assessment matrix for a particular method utilizing a type of database. This study also elucidates the morphology of BT, component extraction, augmentation models, available databases, and classifying between DL, TL, and ML methodologies. Khan et al. [14] focus on this issue by utilizing denoising models and data augmentation on clinical images from 3 diverse databases, improving recognition efficacy. To assess the efficiency of these models, it applies dual DL models employing CNN that established higher precision. Asiri et al. [15] developed an innovative dual-module computerized approach focused on increasing the accuracy and speed of BT recognition. During the Initial stages, the image enhancement model employs a triplet of ML, imaging approaches networks, independent component analysis, and adaptive WF to normalize images and oppose problems like sound and changing lower region dissimilarity. The next module utilizes SVM to validate the output of the initial module.

Schwehr and Achanta [16] introduced the ROI recognition model. It reduces the input size, resulting in a deeper neural network and more aggressive data augmentations. Succeeding the MRI modality pre-processing, fully convolutional AE sectors the diverse brain MRIs that utilize channel-wise self-attention and attention gates. Islam et al. [17] developed a high-accuracy BT detection and classification system utilizing DL models (2D CNN, CNN-LSTM) and ensemble learning on merged MRI datasets. Afroj et al. [18] developed MobDenseNet, a hybrid DL method integrating MobileNet and DenseNet, and compared its performance against popular models, including ResNet101V2, InceptionV3, VGG19, and Xception, for accurate BT classification using MRI data. Joshi et al. [19] proposed TransTopoDx, a novel DL methodology incorporating vision transformers (ViTs) and topological data analysis (TDA) to improve BT diagnosis accuracy, and compares its performance using advanced feature fusion and transfer learning (TL) techniques. Asiri et al. [20] presented an optimized CNN model for BT diagnosis by fine-tuning key hyperparameters, improving classification accuracy and generalization across two benchmark MRI datasets.

Despite advances using DL, TL, and hybrid models like MobDenseNet and TransTopoDx, challenges remain in achieving consistently high accuracy across diverse MRI datasets due to variability in data quality and pre-processing techniques. Many studies concentrate on either segmentation or classification, but integrating both effectively is limited. The research gap is in developing unified models that can robustly handle multi-source data and improve generalization while minimizing computational complexity.

3. PROPOSED METHOD

In this study, we have developed a new EDBT-HDLMSSA technique. The proposed methodology relies on advanced techniques to improve the brain cancer recognition and classification model in biomedical images. The Fig.1 represents the entire procedure of the EDBT-HDLMSSA technique.

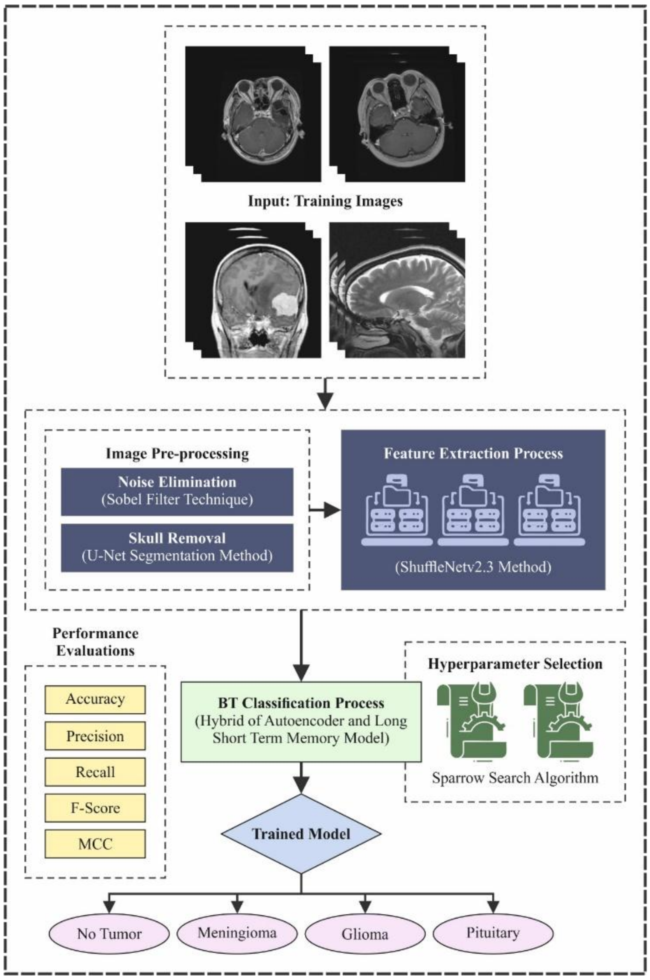

Fig.1. Overall process of EDBT-HDLMSSA technique

3.1 IMAGE PRE-PROCESSING

At first, the image pre-processing stage applies SF to eliminate the noise and skull removal using U-Net segmentation. The SF effectively reduces artefacts while preserving significant image details, crucial for accurate tumour detection. Utilizing U-Net utilizes its robust capability in precise and efficient segmentation, even with limited training data. Compared to conventional methods, U-Net presents superior localization and boundary delineation, enhancing the quality of pre-processed images and ultimately improving downstream classification performance.

The SF is a commonly employed edge detection model in image processing, mainly in medical images for BT recognition [21]. It calculates the gradient of image strength, emphasizing areas with the highest spatial variants, which frequently resemble the edge boundaries of tumours. The filter utilizes dual convolution kernels (vertical and horizontal) to perceive edges in both ways by improving the prospect of tumour margins. In BT segmentation, the SF aids in recognizing tumour boundaries by highlighting intensity variances among normal and abnormal tissues. When combined with DL models, it enhances the extraction of features, helping in precise tumour classification and detection.

The basic structure of U-Net is inspected as a symmetric encoder-decoder network [22]. It mainly contains dual segments: the down-sampling (encoding path) and the up-sampling (decoding path). In the coding path, the input image passes over a sequence of pooling and convolution layers to extract the features and condensation of spatial data. This method permits the system to seize higher-level attributes in the image while decreasing the spatial dimension of the feature mapping. During this decoder path, U-Net accepts the up-sampling process to slowly retrieve the spatial dimension of the feature mapping by transferring the up-sampling or convolution layer. During this procedure, U-Net presents skip connections to connect the feature mapping of the consistent layer in the encoder path to the feature mapping in the decoder path. This model permits the network to preserve more comprehensive information that enhances the precision of the segmentation outcomes. Jump connectivity is one of the advances of U-Net. U-Net can successfully fuse information at various scales by incorporating lower-level and higher-level features. This is particularly significant for edge detection and smaller objective segmentation, as these particulars frequently vanish in down-sampling. Moreover, the jump connection may mitigate the gradient disappearance difficulty, make the method more balanced in training, and enhance convergence speed. In training, U-Net usually utilizes the Dice coefficient loss function or cross-entropy loss function to assess the real label and model output variance. The dice coefficient is particularly appropriate for unstable datasets as it may well reflect the segmentation effect of smaller target regions.

3.2 SHUFFLENETV2.3 MODEL

Besides, the proposed EDBT-HDLMSSA model utilizes the ShuffleNetv2.3 method for feature extraction [23]. This model was chosen for its effectual capability of balancing computational efficiency and accuracy, making it ideal for real-time medical applications. Its lightweight architecture mitigates memory usage and inference time without losing representational capacity. Compared to heavier models, ShuffleNetv2.3 maintains robust feature learning capabilities while being faster and more resource-friendly, which is especially beneficial for deployment in clinical environments with limited hardware.

The ShuffeNetv2.3 model is designated for feature extractor owing to its effective structure that balances computational performance and utilization. Considered especially for resource-constrained and mobile surroundings, it uses the channel shuffle process, which allows lightweight calculations without negotiating precision. The capability of the model to seizure richer feature representations, however, preserves a higher speed of execution, which makes it best for real-world applications. Compared with another DL model, ShuffeNetv2.3 requires lower memory and small parameters, enabling placement in methods with inadequate resources. Besides, its flexibility permits an efficient version through different tasks, enhancing its function in various states. Generally, the ShuffeNetv2.3 model presents a compelling chance for effective and efficient feature extraction. During higher network efficacy similar to ResNeXt and MobileNet, 11 pointwise convolutional captures a massive quantity of computing resources. Problem-based ShuffleNet applies a channel shuffle function to decrease the estimate of 11 pointwise convolutional and combine the data between channels that generate a highly efficient lightweight network. Pooling and convolutional layers usually lengthen the network by stacking, significantly improving recognition precision. On the contrary, this model required to be more stable, which formed minimal accuracy for this model.

ShuffeNet v2 reduces the sum of computations by cleverly using channel shuffling and $shortcut$s. This model generates an optimal balance of speed and accuracy, is greater for systems such as ResNet and Xception, and is highly suitable for mobile applications. Using the ShuffeNetv2 with NN, the ShuffeNet-v2.3 networking architecture was intended to extract adaptive position features. Associated with ShuffeNetv20.5x, ShuffeNetv2.3 changed the sum of block components from the three stages to 13. Therefore, the sum of convolution channels is reduced when it is possible to get the needed precision of the output model. ShuffeNetv2.3 straightforwardly removes the last ReLU in all blocks to solve this problem. Finally, the dropout was applied to stop overfitting. The block component in the ShuffeNetv2.3 networking architecture includes at least 1 ReLU activation function, three convolution layers, and 3 Batch Normalization (BN). Mainly, the 11-convolution layer is applied to decrease the sum of channel sizes and reduce the parameter amounts, improving the capability and nonlinearity to act in addition to data through channels and enhancing the expressivity of systems.

3.3 HYBRID CLASSIFICATION UTILIZING AE-LSTM MODEL

For the BT classification process, the hybrid AE-LSTM technique is employed [24]. This technique is chosen for its ability to effectively capture spatial features through the AE and temporal dependencies via the LSTM network. This integration improves feature representation, sequence learning, and classification accuracy. Compared to standalone CNN or LSTM models, AE-LSTM presents better noise reduction and robust pattern recognition, making it appropriate for intrinsic medical imaging data with subtle discrepancies. The Fig.2 depicts the structure of AE-LSTM.

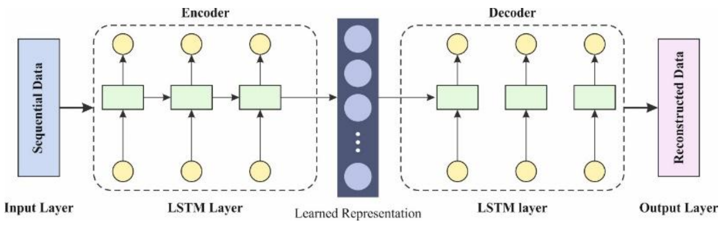

Fig.2. Architecture of AE-LSTM

AE-LSTM networks incorporate LSTM networks and AEs tailored for learning spatial features or temporal dependencies in sequential data. The AE element captures the main features of the input data by learning an effective representation in a compressed variety. In contrast, the LSTM part models the sequence's temporal dynamics and dependencies among frames.

During this AE-LSTM method, the structure comprises dual major modules: the encoder-decoder architecture of the AE and the LSTM layers, which capture temporal relationships among the frames. The AE concentrated on encoding the input data into a low-dimensional latent area. After decoding it, it reverts to the unique input. This procedure assists in removing important features while decreasing dimensionality, which is mainly advantageous for descent recognition in video sequences. The LSTM layers are then utilized to encode the features to capture the serial aspect of the video frames. Dual states occur in the cell. These are New Cell States or new longer-term memory $c(T)$ and New Hidden States or new shorter-term memory $h_{(T)}$. Now is a brief overview of all gates.

3.3.1 Forget Gate:

This gate selects information that must be removed from the cell layer. It utilizes the sigmoid activation function that captures the preceding hidden state $h_{(T\text{-}1)}$ and present state input x_T. The function outputting a value among (0, 1) through zero has been forgotten, and one is preserved.

$$f_1^{(T)} = \sigma\left(W_{fh} \cdot h_{T-1} + W_{fx} \cdot x_T + b_f\right) \quad (1)$$

3.3.2 Primary Input Gate:

The input gate upgrades the new longer-term memory state. The sigmoid activation function is limited in the input gate, whereas the tanh activation function is limited in the input node.

$$i_1^{(T)} = \sigma\left(W_{ih} \cdot h_{T-1} + W_{ix} \cdot x_T + b_i\right) \quad (2)$$

$$g_1^{(T)} = \sigma\left(W_{gh} \cdot h_{T-1} + W_{gx} \cdot x_T + b_g\right) \quad (3)$$

3.3.3 Output Gate:

The LSTM output gate selects which information to utilize further.

$$o_1^{(T)} = \sigma\left(W_{oh} \cdot h_{T-1} + W_{ox} \cdot x_T + b_o\right) \quad (4)$$

The intermediate-level forget, and primary input gates update the new cell State or long-term memory c_T. The LSTM cell state and hidden state equations are in the succeeding methods.

$$c_T = f_T \otimes c_{T-1} + i_T \otimes g_T \quad (5)$$

$$y_T = h_T = o_T \otimes \tanh(c_T) \quad (6)$$

To improve the generalizability of the AE-LSTM method and stop overfitting, dropout layers are combined into the structure. These layers arbitrarily drop particular links in training that assist the method in generalizing unnoticed data well. At last, the model contains a dense layer, which outputs the previous classification.

3.4 PARAMETER SELECTION USING SSA

Finally, the hyperparameter selection of the AE-LSTM model is implemented by utilizing SSA [25]. This model was chosen for its robust global search capability and efficient convergence, which assist in avoiding local minima commonly faced by conventional methods. It effectively balances exploration and exploitation, resulting in optimal hyperparameter tuning. Compared to other optimization algorithms, SSA requires fewer iterations and computational resources, resulting in improved model performance and faster training times.

The SSA model is a swarm intelligence optimizer approach that mimics the sparrow's foraging mechanism. There are three parts to the optimizer method: scout, discoverer, and follower. The discoverer is responsible for searching for the position with enough food in the entire search space and presents a foraging direction or region for each follower. The discoverer is dynamic in the population; given that the sparrow may search for an improved food position, it could become the discoverer. There should be dual states, or each sparrow will transfer to a safer place. Therefore, in all generations of the search, the location of the discoverer is upgraded based on Eq.(7):

$$X_i^{(t+1)} = \begin{cases} X_i^t \cdot \exp\left(\dfrac{-i}{\alpha \cdot T}\right), & R < ST \\ X_i^t + Q \cdot L, & R \geq ST \end{cases} \quad (7)$$

whereas t signifies the present iteration, T represents maximal iteration counts and symbolizes the i^{th} sparrow location at t^{th} iterations. α refers to the randomly generated number inside (0,1), Q denotes a randomly generated number following normal distributions, L symbolizes 1xD matrix, and D means specified size. At the same time, each element has a value of 1, and R($R\in[0,1]$) and ST ($ST\in[0.5,1]$) denote set alarm and security values.

The followers will continuously notice the discoverer's behaviour and modify their location with the discoverer's behaviour; the location of the followers is upgraded as exposed in Eq.(8):

$$X_i^{(t+1)} = \begin{cases} Q \cdot \exp\left(\dfrac{X_{\text{worst}}^t - X_i^t}{i^2}\right), & i > n/2 \\ X_p^{(t+1)} + |\, X_i^t - X_p^{(t+1)} \,| \cdot A^+ \cdot L, & i \leq n/2 \end{cases} \quad (8)$$

where, X_{worst}^t represents the global poor location of the present iteration t, A signifies a 1xD matrix, and its components are randomly given to 1 or -1. A^+ denotes the pseudo-inverse matrix of matrix A. $X_p^{(t+1)}$ stands for the optimal location established by the discoverer.

The scout will understand the danger in the population and, so, fine-tune its complete location in the population of sparrows that is arbitrarily made in the whole population, being responsible for 10% to 20% of the entire population and upgraded as per Eq.(9) which follows:

$$X_{\text{bes}i}^t = \begin{cases} X_{\text{best}}^t + \beta \cdot |\, X_i^t - X_{\text{best}}^t \,|, & f_i > f_g \\ X_i^t + K \cdot \left(\dfrac{|\, X_i^t - X_{\text{worst}}^t \,|}{(f_i - f_\omega) + \varepsilon}\right), & f_i = f_g \end{cases} \quad (9)$$

$X_{\text{bes}i}^t$ signifies the global optimal location, β refers to the step control parameter, K stands for randomly generated number in [1, 1], f_i signifies present individual fitness, and f_g and f_ω denote present global worst and best fitness values. ε means a smaller constant to prevent divide-by-zero error. If $f_g > f_\omega$, it indicates that the sparrow is adjacent to the population and in a safer state, whereas $f_g = f_\omega$, it implies that the sparrow understands the danger and is required to influence other locations.

The SSA originates a fitness function (FF) for attaining an enhanced classification performance. It defines an optimistic number to signify the superior efficiency of the candidate solution. Here, the classifier rate of error reduction was measured as FF. Its mathematical equation is given in Eq.(10).

$$\begin{aligned} \text{fitness}(x_i) &= \text{ClassifierErrorRate}(x_i) \\ &= \frac{\text{Number of Misclassified Samples}}{\text{Total Number of Samples}} \times 100 \end{aligned} \quad (10)$$

4. RESULT ANALYSIS

The performance evaluation of the EDBT-HDLMSSA method is studied under the BT MRI dataset [26]. The technique is simulated using Python 3.6.5 on a PC with an i5-8600k, 250GB SSD, GeForce 1050Ti 4GB, 16GB RAM, and 1TB HDD. Parameters include a learning rate of 0.01, ReLU activation, 50 epochs, 0.5 dropouts, and a batch size of 5. This dataset contains 7013 images under four classes, namely No tumour, Meningioma, Glioma, and Pituitary, as depicted in Table.1.

Table.1. Details of dataset

Classes	No. of Images
No Tumor	1992
Meningioma	1644
Glioma	1621
Pituitary	1756
Total Images	7013

The Fig.3 established the classifier outcomes of the EDBT-HDLMSSA methodology. The Figs. 3a-3b displays the confusion matrices with correct recognition of every class below 70%TRPH and 30%TSPH. The Fig.3c exhibits the PR analysis, representing superior performance over all class labels. This is followed by Fig.3d, which establishes the analysis of ROC, establishing capable results with higher ROC analysis for dissimilar classes.

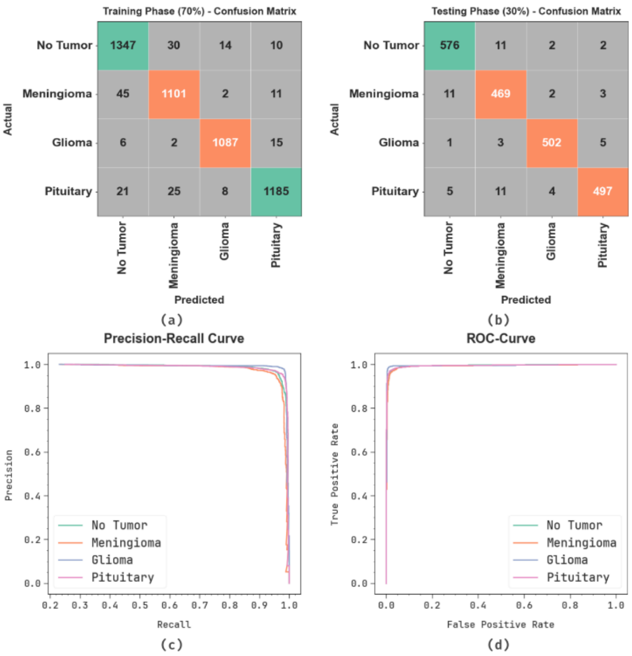

Fig.3. Classifier outcomes of (a-b) confusion matrix and (c-d) curves of PR and ROC

The Table.2 and Fig.4 signify the BT detection of the EDBT-HDLMSSA approach under 70%TRPH and 30%TSPH. The result stated that the EDBT-HDLMSSA approach has properly classified each dissimilar class label. Based on 70% TRPH, the proposed EDBT-HDLMSSA technique gains an average $accu_y$ of 98.07%, $prec_n$ of 96.22%, $reca_l$ of 96.18%, F_{score} of 96.20%, and MCC of 94.91%. Additionally, depending on 30% TSPH, the proposed EDBT-HDLMSSA technique achieves an average $accu_y$ of 98.57%, $prec_n$ of 97.13%, $reca_l$ of 97.13%, F_{score} of 97.13%, and MCC of 96.18%.

Table.2. BT Detection of EDBT-HDLMSSA Model under 70%TRPH And 30%TSPH

Class	$Accu_y$	$Prec_n$	$Reca_l$	F_{score}	MCC
TRPH (70%)					
No Tumor	97.43	94.93	96.15	95.53	93.74
Meningioma	97.66	95.08	95.00	95.04	93.50
Glioma	99.04	97.84	97.93	97.88	97.27
Pituitary	98.17	97.05	95.64	96.34	95.12
Average	98.07	96.22	96.18	96.20	94.91
TSPH (30%)					
No Tumor	98.48	97.13	97.46	97.30	96.24
Meningioma	98.05	94.94	96.70	95.81	94.55
Glioma	99.19	98.43	98.24	98.33	97.80
Pituitary	98.57	98.03	96.13	97.07	96.14
Average	98.57	97.13	97.13	97.13	96.18

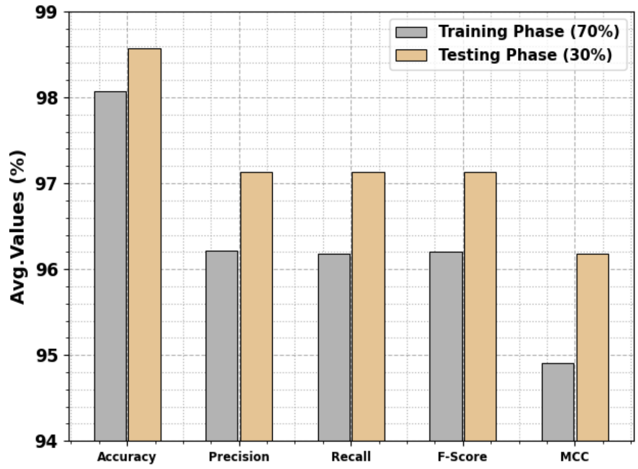

Fig.4. Average of EDBT-HDLMSSA model under 70%TRPH and 30%TSPH

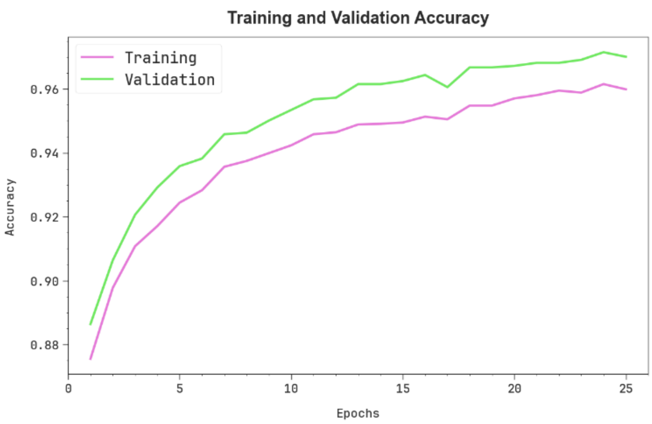

Fig.5. $Accu_y$ curve of EDBT-HDLMSSA model

The Fig.5 illustrates the training (TRA) $accu_y$ and validation (VAL) $accu_y$ analysis of the EDBT-HDLMSSA methodology. The $accu_y$ analysis is calculated within the range of 0-25 epochs. The outcome highlights that the TRA and VAL $accu_y$ analysis exhibited an increasing trend, which informed the capacity of the EDBT-HDLMSSA technique with superior performance across multiple iterations. Simultaneously, the TRA and VAL $accu_y$ leftovers closer across the epochs, which specifies inferior overfitting and exhibits maximum outcomes of the EDBT-HDLMSSA methodology, ensuring continuous prediction on unseen samples.

The Fig.6 shows the TRA loss (TRALOS) and VAL loss (VALLOS) curves of the EDBT-HDLMSSA method. The loss values are computed across an interval of 0-25 epochs. It is denoted that the TRALOS and VALLOS analysis exemplify a diminishing trend, notifying the capacity of the EDBT-HDLMSSA approach in balancing a trade-off between simplification and data fitting. The constant reduction in loss values guarantees the maximal outcomes of the EDBT-HDLMSSA and tunes the prediction results over time.

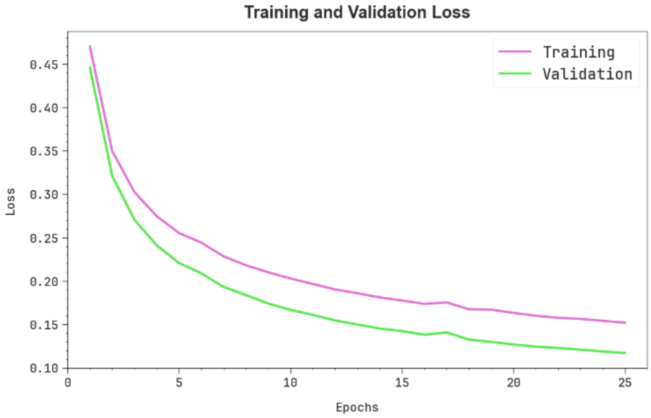

Fig.6. Loss analysis of EDBT-HDLMSSA technique

The comparison analysis of the EDBT-HDLMSSA approach with existing methodologies is illustrated in Table.3 and Fig.7 [18-19, 27-29]. The EDBT-HDLMSSA approach outperforms by presenting superior overall performance. It achieves an impressive $accu_y$ of 98.57%, with precision, recall, and F-score all reaching 97.13%. This demonstrates its balanced and robust capability in classification tasks. Compared to other models, the EDBT-HDLMSSA method presents a significant improvement in both efficiency and reliability.

Table.3. Comparison outcome of the EDBT-HDLMSSA approach with existing models [18-19, 27-29]

Model	$Accu_y$	$Prec_n$	$Recal$	F_{score}
InceptionV3	97.12	91.57	94.24	91.68
ResNet50 Model	96.97	91.86	96.39	96.84
Xception Model	95.67	93.33	92.77	90.43
MobileNetV2	95.45	92.75	96.09	94.85
CNN-SVM-kNN	97.00	92.16	93.84	91.00
GAN Algorithm	96.25	90.71	90.69	96.71
MANet Model	97.71	96.79	92.05	93.21
VGG-16 Model	96.00	91.66	90.60	92.26
ResNet101V2	96.06	94.22	91.15	93.24
DenseNet	98.00	92.02	94.16	90.51
ViT	97.59	91.17	92.10	93.96
EDBT-HDLMSSA	98.57	97.13	97.13	97.13

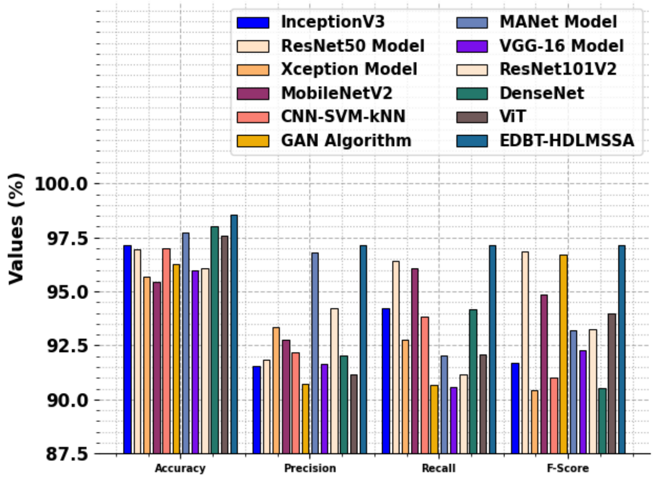

Fig.7. Comparison outcome of EDBT-HDLMSSA approach with existing models

The computational time analysis of the EDBT-HDLMSSA method with existing models is shown in Table 4 and Fig.8. The EDBT-HDLMSSA method exhibits the fastest CT among all evaluated models, completing tasks in just 6.11 seconds. This is significantly quicker compared to other well-known models such as InceptionV3 with 22.67 seconds, ResNet50 with 15.04 seconds, and MobileNetV2 with 24.81 seconds. The efficient CT of EDBT-HDLMSSA model highlights its suitability for real-time or resource-constrained applications, presenting a valuable balance between speed and performance.

Table.4. CT analysis of the EDBT-HDLMSSA method with existing models [18-19, 27-29]

Model	CT (sec)
InceptionV3	22.67
ResNet50 Model	15.04
Xception Model	16.49
MobileNetV2	24.81
CNN-SVM-kNN	10.22
GAN Algorithm	12.85
MANet Model	9.61
VGG-16 Model	24.40
ResNet101V2	13.66
DenseNet	11.23
ViT	15.51
EDBT-HDLMSSA	6.11

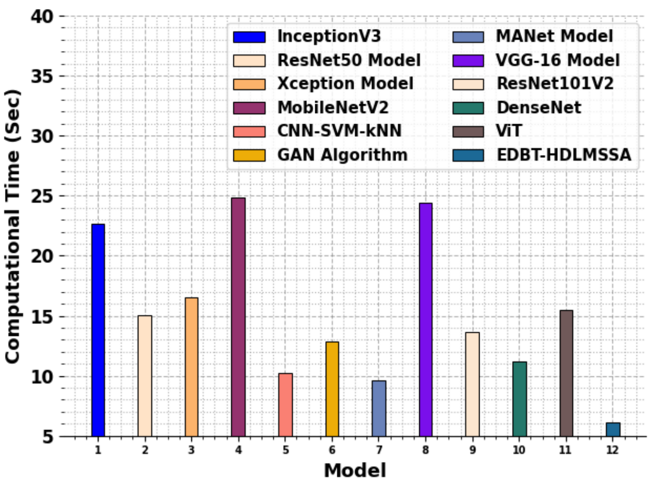

Fig.8. CT analysis of EDBT-HDLMSSA method with existing models

5. CONCLUSION

In this paper, we have developed a new EDBT-HDLMSSA technique. The proposed EDBT-HDLMSSA technique relies on improving the brain cancer recognition and classification model in biomedical images using advanced techniques. At first, the image pre-processing stage applies SF to eliminate the noise and skull removal using U-Net segmentation. Besides, the proposed EDBT-HDLMSSA model designs the ShuffleNetv2.3 method for extracting feature models. For the BT classification process, the hybrid AE-LSTM technique is deployed. Eventually, the hyperparameter selection of the AE-LSTM model is implemented by the design of the SSA. A wide range of experiments was conducted to validate the performance of the EDBT-HDLMSSA technique. The outcomes specified that the EDBT-HDLMSSA model emphasized improvement over other existing methods.

REFERENCES

[1] T. Hossain, F.S. Shishir, M. Ashraf, M.A. Al Nasim and F.M. Shah, "Brain Tumor Detection using Convolutional Neural Network", *Proceedings of the International Conference on Advances in Science, Engineering and Robotics Technology*, pp. 1-6, 2019.

[2] J. Amin, M. Sharif, M. Raza, T. Saba and M.A. Anjum, "Brain Tumor Detection using Statistical and Machine Learning Method", *Computer Methods and Programs in Biomedicine*, Vol. 177, pp. 69-79, 2019.

[3] P.M. Shakeel, T.E.E. Tobely, H. Al-Feel, G. Manogaran and S. Baskar, "Neural Network based Brain Tumor Detection using Wireless Infrared Imaging Sensor", *IEEE Access*, Vol. 7, pp. 5577-5588, 2019.

[4] A. Chattopadhyay and M. Maitra, "MRI-based Brain Tumour Image Detection using CNN based Deep Learning Method", *Neuroscience Informatics*, Vol. 2, No. 4, pp. 1-6, 2022.

[5] M.S. Alam, M.M. Rahman, M.A. Hossain, M.K. Islam, K.M. Ahmed, K.T. Ahmed, B.C. Singh and M.S. Miah, "Automatic Human Brain Tumor Detection in MRI Image using Template-based K Means and Improved Fuzzy C Means Clustering Algorithm", *Big Data and Cognitive Computing*, Vol. 3, No. 2, pp. 1-18, 2019.

[6] M.O. Khairandish, M. Sharma, V. Jain, J.M. Chatterjee and N.Z. Jhanjhi, "A Hybrid CNN-SVM Threshold Segmentation Approach for Tumor Detection and Classification of MRI Brain Images", *IRBM*, Vol. 43, No. 4, pp. 290-299, 2022.

[7] S. Sajid, S. Hussain and A. Sarwar, "Brain Tumor Detection and Segmentation in MR Images using Deep Learning", *Arabian Journal for Science and Engineering*, Vol. 44, pp. 9249-9261, 2019.

[8] J. Seetha and S.S. Raja, "Brain Tumor Classification using Convolutional Neural Networks", *Biomedical and Pharmacology Journal*, Vol. 11, No. 3, pp. 1-9, 2018.

[9] M.K. Abd-Ellah, A.I. Awad, A.A. Khalaf and H.F. Hamed, "A Review on Brain Tumor Diagnosis from MRI Images: Practical Implications, Key Achievements and Lessons Learned", *Magnetic Resonance Imaging*, Vol. 61, pp. 300-318, 2019.

[10] N.N. Mostafa, "Human Brain Tumors Detection using Neutrosophic C-Means Clustering Algorithm", *Full Length Article*, Vol. 1, No. 1, pp. 1-11, 2023.

[11] A.B. Abdusalomov, M. Mukhiddinov and T.K. Whangbo, "Brain Tumor Detection based on Deep Learning Approaches and Magnetic Resonance Imaging", *Cancers*, Vol. 15, No. 16, pp. 1-29, 2023.

[12] R. Poonguzhali, S. Ahmad, P.T. Sivasankar, S.A. Babu, P. Joshi, G.P. Joshi and S.W. Kim, "Automated Brain Tumor Diagnosis using Deep Residual U-Net Segmentation Model", *Computers, Materials and Continua*, Vol. 74, No. 1, pp. 2179-2194, 2023.

[13] S. Solanki, U.P. Singh, S.S. Chouhan and S. Jain, "Brain Tumor Detection and Classification using Intelligence Techniques: an Overview", *IEEE Access*, Vol. 11, pp. 12870-12886, 2023.

[14] M.F. Khan, A. Iftikhar, H. Anwar and S.A. Ramay, "Brain Tumor Segmentation and Classification using Optimized Deep Learning", *Journal of Computing and Biomedical Informatics*, Vol. 7, No. 1, pp. 632-640, 2024.

[15] A.A. Asiri, T.A. Soomro, A.A. Shah, G. Pogrebna, M. Irfan and S. Alqahtani, "Optimized Brain Tumor Detection: A Dual-Module Approach for MRI Image Enhancement and Tumor Classification", *IEEE Access*, Vol. 12, pp. 42868-42887, 2024.

[16] Z. Schwehr and S. Achanta, "Brain Tumor Segmentation based on Deep Learning, Attention Mechanisms and Energy-based Uncertainty Predictions", *Multimedia Tools and Applications*, pp. 1-20, 2025.

[17] M.N. Islam, M.S. Azam, M.S. Islam, M.H. Kanchan, A.S. Parvez and M.M. Islam, "An Improved Deep Learning-based Hybrid Model with Ensemble Techniques for Brain Tumor Detection from MRI Image", *Informatics in Medicine Unlocked*, Vol. 47, pp. 1-15, 2024.

[18] M. Afroj, M.R.H. Mondal, M.R. Hassan and S. Akter, "MobDenseNet: A Hybrid Deep Learning Model for Brain Tumor Classification using MRI", *Array*, Vol. 26, pp. 1-12, 2025.

[19] D. Joshi, B.K. Singh, K.K. Nagwanshi and N.S. Choubey, "Enhanced Brain Tumor Diagnosis using Transfer Learning

with Vision Transformers and Topological Data Analysis", *Procedia Computer Science*, Vol. 258, pp. 4048-4059, 2025.

[20] A.A. Asiri, A. Shaf, T. Ali, M. Aamir, M. Irfan and S. Alqahtani, "Enhancing Brain Tumor Diagnosis: An Optimized CNN Hyperparameter Model for Improved Accuracy and Reliability", *PeerJ Computer Science*, Vol. 11, pp. 123080-123095, 2024.

[21] M. Lecca and R.P. Serapioni, "Non-Uniformly Lighted Image Enhancement Exploiting the Atangana-Baleanu Fractional Integral and the Sobel Filter", *Journal of the Optical Society of America A*, Vol. 42, No. 2, pp. 183-192, 2025.

[22] Z. Wang, Y. Chen, F. Wang and Q. Bao, "Improved Unet Model for Brain Tumor Image Segmentation based on ASPP-Coordinate Attention Mechanism", *Proceedings of the International Conference on Big Data and Artificial Intelligence and Software Engineering*, pp. 393-397, 2024.

[23] M. Ragab, B.M. Alghamdi, R. Alakhtar, H. Alsobhi, L.A. Maghrabi, G. Alghamdi, S. Nooh and A.L. Abdullah, "Enhancing Cybersecurity in Higher Education Institutions using Optimal Deep Learning-based Biometric Verification", *Alexandria Engineering Journal*, Vol. 117, pp. 340-351, 2025.

[24] S. Chakraborty and M. Ghosh, "Enhanced Vision-based Human Fall Detection with Mask-RCNN and Autoencoder-LSTM Hybrid Framework", *Proceedings of the International Sixth Doctoral Symposium on Intelligence Enabled Research*, pp. 1-8, 2025.

[25] P. Wang, T. Feng, C. Song, J. Li and S.X. Yang, "A Study of the Stability of an Industrial Robot Servo System: PID Control based on a Hybrid Sparrow Optimization Algorithm", *Actuators*, Vol. 14, No. 2, pp. 1-17, 2025.

[26] "Brain Tumor MRI Datase", Available at https://www.kaggle.com/datasets/masoudnickparvar/brain-tumor-mri-dataset, Accessed in 2021.

[27] M.A. Gomez-Guzman, L. Jimenez-Beristaín, E.E. García-Guerrero, O.R. Lopez-Bonilla, U.J. Tamayo-Perez, J.J. Esqueda-Elizondo, K. Palomino-Vizcaino and E. Inzunza-Gonzalez, "Classifying Brain Tumors on Magnetic Resonance Imaging by using Convolutional Neural Networks", *Electronics*, Vol. 12, No. 4, pp. 1-22, 2023.

[28] J. Jain, M. Kubadia, M. Mangla and P. Tawde, "Comparison of Transfer Learning Techniques to Classify Brain Tumours using MRI Images", *Engineering Proceedings*, Vol. 59, No. 1, pp. 1-9, 2024.

[29] A.A. Asiri, A. Shaf, T. Ali, U. Shakeel, M. Irfan, K.M. Mehdar, H.T. Halawani, A.H. Alghamdi, A.F.A. Alshamrani and S.M. Alqhtani, "Exploring the Power of Deep Learning: Fine-Tuned Vision Transformer for Accurate and Efficient Brain Tumor Detection in MRI Scans", *Diagnostics*, Vol. 11, pp. 1-17, 2023.